frontiers | Frontiers in Earth Science

ORIGINAL RESEARCH
published: 11 April 2022
doi: 10.3389/feart.2022.883146

Geochemical and Geological Characterization of Upper Permian Linghao Formation Shale in Nanpanjiang Basin, SW China

*Yifan Gu[1,2], Guangyin Cai[1,2], Dongfeng Hu[3], Zhihong Wei[3], Ruobing Liu[3], Jing Han[3], Zhiwei Fan[3], Jingyu Hao[3] and Yuqiang Jiang[1,2]**

[1]School of Geoscience and Technology, Southwest Petroleum University, Chengdu, China, [2]PetroChina Key Laboratory of Unconventional Oil and Gas Resources, The Unconventional Reservoir Evaluation Department, Chengdu, China, [3]Exploration Company, Sinopec, Chengdu, China

The Upper Permian Linghao Formation shale is the most potential shale gas exploration target in Nanpanjiang Basin. In this study, X-ray diffraction, field emission scanning electron microscopy, CH4 isothermal adsorption, and nuclear magnetic resonance cryoporometry are intergrated to reveal comprehensive characterization of Linghao Formation shale collected from a well in Nanpanjiang Basin. Results indicate that organic-rich shales developed in the Ling 1 member and the lower part of Ling 3 member. The organic-rich shales are predominantly characterized by kerogen type I, with a relatively highly mature to overmature status. The Ling 1 organic-rich shale mainly consists of mixed shale lithofacies, and the organic-rich shale in the lower part of Ling 3 is mainly composed of argillaceous shale. The pore volume in Ling 1 organic-rich shale is mainly contributed by 3- to 6-nm and 8- to 11-nm organic pores. The pore volume of Ling 3 organic-rich shale is mainly contributed by 2- to 3-nm and 4- to 11-nm organic pores. The organic pores between 3 and 10 nm also have a small contribution to the pore volume. The absolute adsorption gas content of Ling 1 and Ling 3 organic-rich shale is 1.21 m^3/t and 1.64 m^3/t, respectively. The absolute adsorption gas content of Ling 1 and Ling 3 organic-rich shale exceeds the minimum standard for commercial shale gas development in China (1.0 m^3/t). According to the adsorption gas ratio of 50%, the total gas content of Ling 1 and Ling 3 organic-rich shale can reach 3.28 m^3/t and 2.28 m^3/t, respectively. It is suggested that the Upper Permian Linghao Formation shale in the Nanpanjiang Basin has a significant potential for shale gas exploration.

Keywords: Upper Permian, shale lithofacies, geochemistry, organic-rich shale, Linghao Formation, Nanpanjiang Basin

OPEN ACCESS

Edited by:
Shu Jiang,
The University of Utah, United States

Reviewed by:
Mengdi Sun,
Northeast Petroleum University, China
Zhaodong Xi,
China University of Geosciences, China
Chenggong Zhang,
Chengdu University of Technology, China

****Correspondence:***
Yuqiang Jiang
xnsyjyq3055@126.com

Specialty section:
This article was submitted to Economic Geology, a section of the journal Frontiers in Earth Science

Received: *24 February 2022*
Accepted: *14 March 2022*
Published: *11 April 2022*

Citation:
Gu Y, Cai G, Hu D, Wei Z, Liu R, Han J, Fan Z, Hao J and Jiang Y (2022) Geochemical and Geological Characterization of Upper Permian Linghao Formation Shale in Nanpanjiang Basin, SW China. Front. Earth Sci. 10:883146. doi: 10.3389/feart.2022.883146

INTRODUCTION

The great success of shale gas development in North America has triggered a boom in shale gas exploration and promoted research on the potential of global shale gas development (Curtis, 2002; Li et al., 2007; Zou et al., 2010; Clarkson et al., 2012; Zou et al., 2015). Most of the recovered shale gas in the United States is produced from marine shales (Wei et al., 2020). China has developed three types of organic shale: one is the marine shale of Early Paleozoic, the second is the Carboniferous-Permian

transitional shale, and the third is the Mesozoic lacustrine shale (Bao et al., 2016; Xi et al., 2017; Liang et al., 2018; Kuang et al., 2020; Liu et al., 2021; Wang et al., 2022). In 2010, the exploration and development of Silurian marine shale gas in China made an industrial breakthrough (Zou et al., 2010; Qiu and Zou, 2020; Zhang et al., 2022), which has been more than 12 years ago, and the annual output in 2018 reached $10.8 \times 109\ m^3$ (Qiu and Zou, 2020). Under this demonstration effect, marine shales of other strata in China have quickly become the key targets of shale gas exploration and evaluation (Wei et al., 2012; Cao et al., 2015; Ding et al., 2018; Wang et al., 2018; Zhang et al., 2019a; Zhang et al., 2019b; Zou et al., 2019; Zhang et al., 2020a; Zhang et al., 2020b; Ding et al., 2021), but they are still in the early stages of exploration and have not made any industrial breakthroughs. The Sichuan Basin and the Nanpanjiang Basin are the two largest oil- and gas-bearing basins in south China. A number of Permian marine or marine-continental transitional organic-rich shale units are recognized (Han et al., 2017; Guo et al., 2018; Chen et al., 2020; He et al., 2020; Zhu et al., 2021), which play the role of source rock covering conventional natural gas production. In recent years, the research achievements of Permian shale in Sichuan Basin are abundant (Han et al., 2017; Guo et al., 2018; Zhang et al., 2018; Sun et al., 2020; Wang et al., 2021), but a relevant study of Nanpanjiang Basin is rare.

Previous studies have shown that the Permian organic-rich shales developed in the Nanpanjiang Basin met the conditions for the accumulation of shale gas (Liu et al., 2018; Luo et al., 2018; He et al., 2020). However, due to the rapid change of the sedimentary environment, the Upper Permian organic-rich shale in different areas of the Nanpanjiang Basin varies greatly in terms of shale thickness, geochemical characteristics, hydrocarbon generation capacity, mineral composition, and gas content (Liu et al., 2018; Luo et al., 2018). At present, there are many views about the exploration and evaluation of Permian shale in the Nanpanjiang Basin (Sun et al., 2019; He et al., 2020). Luo et al. (2018) studied the geological and geochemical characteristics of the Upper Permian organic-rich shale under transitional environment; they presented that the high TOC value, high thermal maturity level, and moderate burial depth are favorable factors for shale gas exploration. However, the high clay content is not conducive to shale gas development. He et al. (2020) pointed out that the organic matter of the Upper Permian organic-rich shale in Nanpanjiang Basin was primarily sourced from terrestrial plants, and the detrital flux and paleoproductivity may play a limited role on organic matter accumulation. Liu et al. (2018) proposed that detrital influx decreased the concentration of TOC in the Upper Permian organic-rich shale of Nanpanjiang Basin, and paleoproductivity is not the critical factor controlling the concentration of TOC. In this study, X-ray diffraction (XRD) analysis, field emission scanning electron microscopy (FE-SEM), CH_4 isothermal adsorption, and nuclear magnetic resonance (NMR) cryoporometry are intergrated to reveal comprehensive characterization of Upper Permian Linghao Formation organic-rich shale collected from the studied well in Nanpanjiang Basin. It might produce valuable information for engineers to properly evaluate the storage capacity and exploration potential of Upper Permian organic-rich shale. It is hoped that this study will contribute to the industrial breakthrough of shale gas exploration in Nanpanjiang Basin.

GEOLOGICAL SETTING

The Nanpanjiang Basin, with an area of 380, 000 km^2, is located at the junction of Yunnan, Guizhou, and Guangxi, and the geotectonic position is located in the southwestern margin of the South China Block (Xia et al., 2018) (**Figure 1A**). Similar to the Carboniferous Datang Formation in Nanpanjiang Basin, the Linghao Formation is a special and representative stratigraphic unit formed by the deep water sedimentary environment between isolated platforms during late Permian (Zhang et al., 2012b; Zhang et al., 2012c). Observations from the studied well and outcrops show that the Linghao Formation is in conformable contact with underlying limestone or muddy limestone of Maokou Formation, and overlying Luolou Formation. According to the combination of lithology and logging characteristics, the Linghao Formation can be divided into Ling 1 member, Ling 2 member, and Ling 3 member. The Ling 1 member consists of shale with Emeishan basalt interbed. Previous studies suggested that the influence of igneous rocks including basalt on the sedimentary organic matter is characterized by organic matter maturity in advance and the maturity is abnormally high (Simoneit et al., 1978; Alalade and Tyson, 2013). The Ling 2 member is composed of mudstone and limestone. The Ling 3 member is composed of shale (**Figure 1B**). According to previous studies, the northwest Nanpanjiang Basin is dominated by swamp, tidal flat, and lagoon facies during Linghao period (Luo et al., 2018; He et al., 2020). The contemporaneous strata of the Linghao period comprises mudstones, silty mudstones, siltstones, limestones, and coals (He et al., 2020). The studied well is located in central Nanpanjiang Basin which is dominated by shelf or deep water basin facies during Linghao period (**Figure 1A**).

SAMPLES AND METHODS

The studied well carried out continuous coring in the Permian Linghao Formation. Core observation identified different lithology, including shale, organic-rich shale, fine-grained sandstone, siltstone, silty mudstone, limestone, chert, and record the lithology combination of different members. Overall, 300 thin sections of core samples were made, and the core observation results were further verified by a Carl Zeiss microscope digital photography system under transmitted light. Full combustion of shale samples were done under high temperature and pure oxygen flow. Then strong oxidant was used to react in acidic solution, and the collected carbon dioxide gas was purified in a vacuum system to remove the interference. The content of carbon dioxide gas was measured by an Elementar VarioMACRO CHNS element analyzer, and the content of organic carbon was calculated. The bulk mineralogical compositions of 59 selected samples were analyzed by XRD using a Panalytical X'Pert PRO MPD X-ray diffractometer.

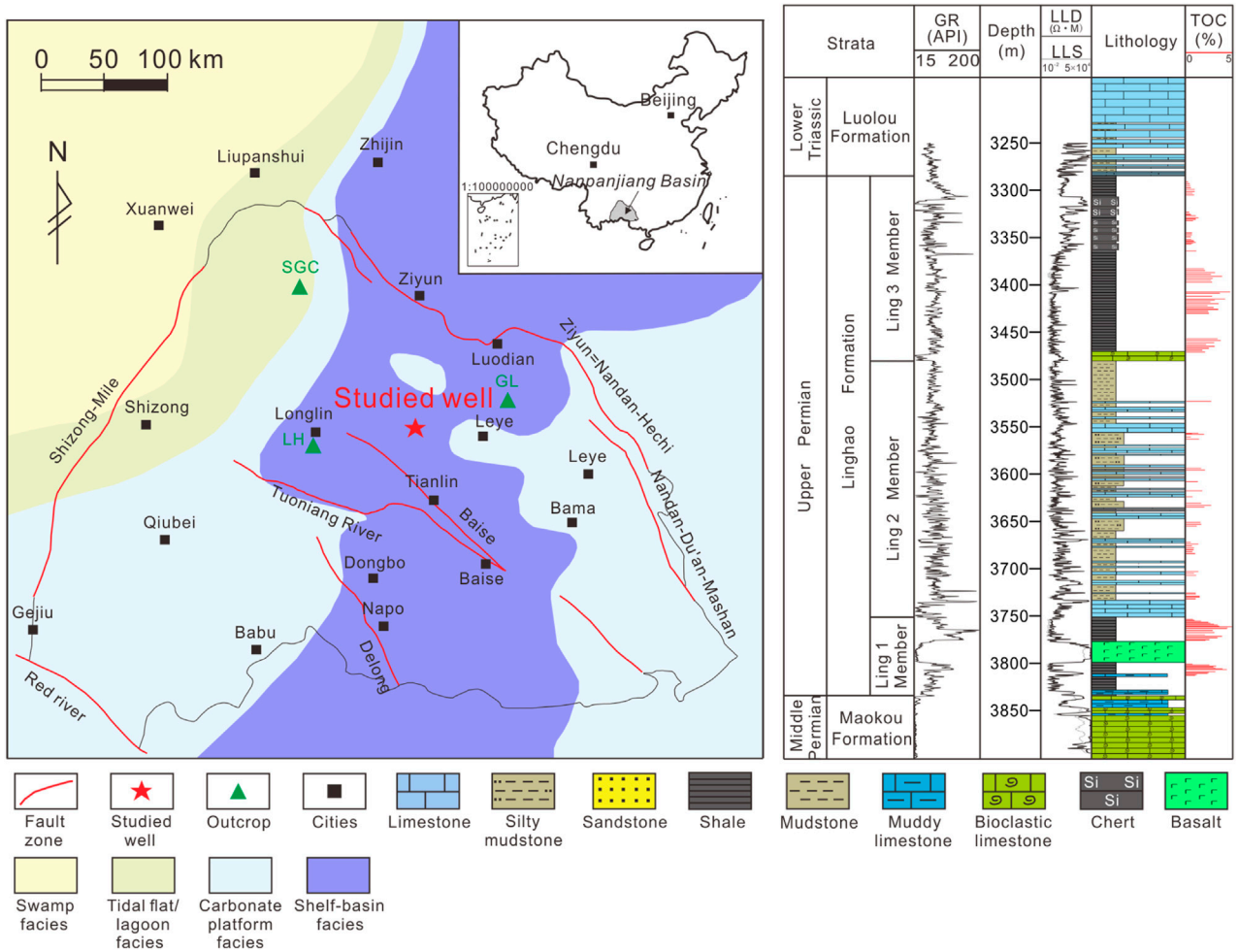

FIGURE 1 | (A) Location of the Nanpanjiang Basin, Southwest China (modified from Xia et al., 2018). **(B)** Generalized stratigraphy of Upper Permian Linghao Formation in the study area (based on the studied well).

The samples were ground into powder (>200 mesh), and then step-scanned at a rate of 2°/min from 5° to 75° (2θ). Before high-resolution SEM observation, the selected shale samples are cut into a 1.5-cm length, 1.0-cm width, and 0.5-cm height cube (perpendicular to the bedding plane) and then polished by argon ion. After the treatment, the FEI-QUANTAN 250 FE-SEM was used to image the micropores in shale. The resolution can reach to 0.8 nm, with a 20,000–300,00× magnification at an acceleration voltage adjustment of 0.02–30 kV. The built-in algorithm of "ImageJ" software was used to quantitatively obtain microfractures, organic pores, and inorganic pores.

In this work, based on the second electron imaging observation on the polished surface of the shale sample, nanoscale pores can be imaged by optimizing the acceleration voltage and scanning speed of the working state. Using the NMRC12-010V NMR instrument produced by Niumag Company, low-temperature NMR cryoporometry was carried out on the Linghao Formation samples. First, the samples were mechanically crushed to 35–50 meshes and then dried in a vacuum drying oven at 373.15 K for 24 h. However, the samples were packed into 2-ml chromatographic bottle and vacuumed for 12 h, and then pure water was added, balanced for 6 h, and centrifuged for 12 h. Finally, the samples were packed in a 25-ml chromatographic bottle and placed in the coil of the instrument for testing. Porosity values are tested by an NMRC12-010V NMR instrument to make shale samples into 2.5-cm × 4-cm plug. Before the test, the plug samples were placed in a vacuum drying oven at 373.15 K for 24 h, and then vacuumed, with 30 MPa pressure saturated water for 12 h. After the saturation is completed, the plug samples were placed in the coil to start the test. Methane isothermal adsorption experiment was carried out using Rubotherm high-temperature and high-pressure gravimetric adsorption instrument produced in the Netherlands. The experimental temperature was set to 110°C, and the pressure was from 0.5 to 30 MPa. The actual formation conditions of 30 MPa and 110°C are basically the same as those of the studied wells. The adsorption phase

TABLE 1 | Key parameters of major gas shale in America and the Linghao Formation shale (modified from Luo et al., 2018).

Shale name	Burial depth (m)	TOC (%)	Ro (%)	Kerogen type	Porosity (%)
Ling 1	3,753–3,820	0.84–4.12	3.49–4.17	I	0.11–1.01 (average 0.52)
Ling 2	3,481–3,732	0.50–3.08	3.39–3.93	I	0.17–2.26 (average 1.22)
Ling 3	3,291–3,471	0.24–4.36	3.38–4.13	I	0.83–1.07 (average 0.95)
Longtan	1,300–2,500	0.35–26.99	1.10–2.74	III	1.39–5.05
Barnett	1981–2,591	2.00–7.00	1.10–2.20	II	4.00–5.00
Lewis	914–1829	0.45–2.50	1.60–1.88	I	3.00–5.50
New Albany	183–1,494	1.00–25.00	0.40–1.00	II	10.00–14.00

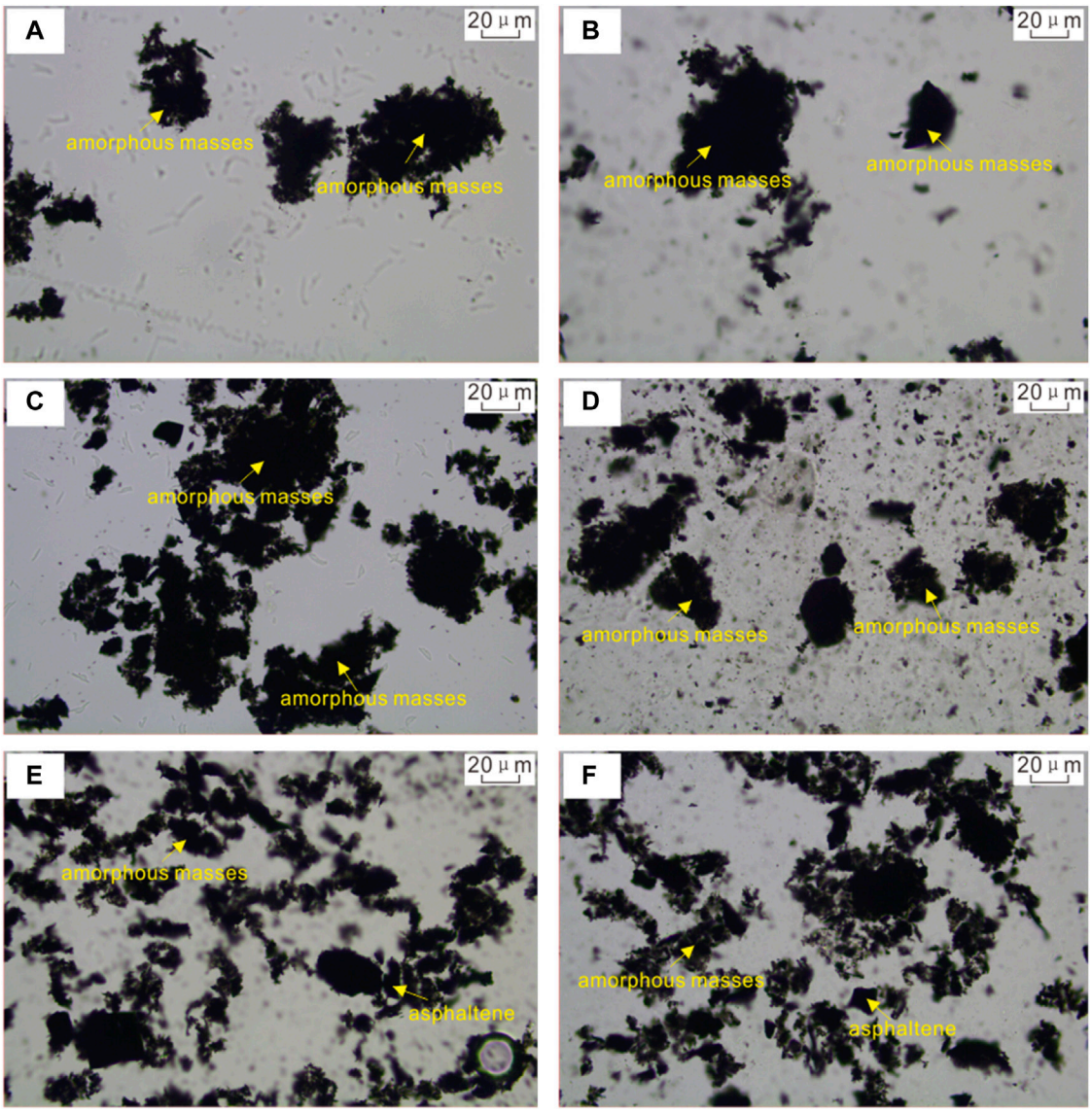

FIGURE 2 | Kerogen maceral for the Upper Permian Linghao Formation shale/mudstone from the studied well in Nanpanjiang Basin. **(A)** Amorphous masses, Ling 1 member organic-rich shale, 3,767.54 m. **(B)** Amorphous masses, Ling 1 member organic-rich shale, 3,772.24 m. **(C)** Amorphous masses, Ling 2 member mudstone, 3,557.75 m. **(D)** Amorphous masses, Ling 2 member mudstone, 3561 m. **(E)** Amorphous masses and asphaltene, Ling 3 member organic-rich shale, 3,408.92 m. **(F)** Amorphous masses and asphaltene, Ling 3 member organic-rich shale, 3,412.12 m.

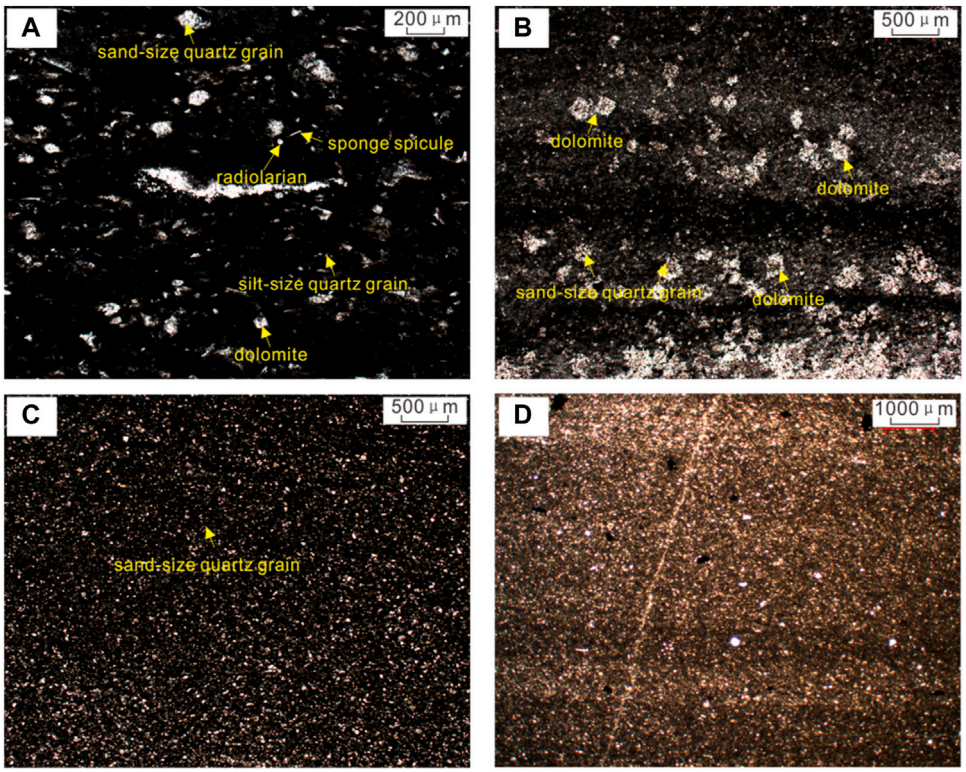

FIGURE 3 | Thin section photomicrograph for the Upper Permian Linghao Formation shale/mudstone from the studied well in Nanpanjiang Basin. **(A)** Thin section image (transmitted light) showing the presence of sponge spicule, radiolarian, silt size quartz grains, sand size quartz grains, and dolomite grains in organic-rich shale, Ling 1 member, 3,773.11 m. **(B)** Thin section image (transmitted light) showing the presence of sand size quartz grains and dolomite grains in mudstone, Ling 2 member, 3,556.10 m. **(C)** Organic-rich shale containing sand size quartz grains, Ling 3 member, 3,414.88 m. **(D)** Shale containing sand size quartz grains, Ling 3 member, 3310 m.

density was obtained by fitting calculation, and the ternary Langmuir equation was used to fit excess adsorption and absolute adsorption.

RESULTS AND DISCUSSION

Organic Geochemistry and Mineral Compositions

Geochemical indicators for characterizing and evaluating shale gas reservoirs include total organic carbon (TOC), maturity (Ro), kerogen type, hydrocarbon phase, gas content, and composition (Zou et al., 2015; Zou et al., 2019). According to the marine shale data (Zou et al., 2015; Zhou et al., 2016; Xi et al., 2018; Zou et al., 2019; Xi et al., 2022), the higher the organic matter content, the greater the gas potential of shale. In addition, shale gas can be adsorbed on the surface of organic matter. Under certain pressure conditions, the higher the organic matter content, the greater the adsorption capacity of shale gas (Curtis, 2002; Li et al., 2007). TOC can also have a decisive influence on the gas sorption capacity of the shale (Ross and Bustin, 2009). Higher TOC content implies higher hydrocarbon generation potential and better adsorption capacity for shale gas. Currently, the lower limit of TOC for commercial exploitation of shale gas is generally 2.0%. However, a few scholars suggested that the lower limit of TOC of shale with a high-maturity stage can be reduced to 1% (Curtis, 2002; Jarvie et al., 2007; Zou et al., 2010). The analysis results of the TOC content in Linghao Formation showed that the TOC content varied greatly in different members, with the overall range of 0.24–4.36%, and the average value of 1.95%. Among them, Ling 1 member is 0.84–4.12%, with an average of 2.58%. The TOC distribution of Ling 2 member is 0.50–3.08% (**Table 1**), with an average of 1.52%. The TOC distribution of Ling 3 member is 0.24–4.36%, with an average of 1.85%. The organic-rich shale is distributed in the Ling 1 member and lower part of Ling 3 member (**Figure 1B**).

Thermal maturity is another important parameter for evaluating shale reservoirs. It affects not only gas generation potential but also gas adsorption capacity (Nie et al., 2009; Zhang et al., 2020c). With the increase in thermal maturity, the hydrocarbon generation potential decreases, but the gas adsorption capacity increases. Vitrinite reflectance is the most reliable organic matter maturity index, which is widely used to characterize the organic matter maturity of shale. The organic-rich shale of the Linghao Formation in the study area lacks vitrinite (**Figures 2A,B**) but generally

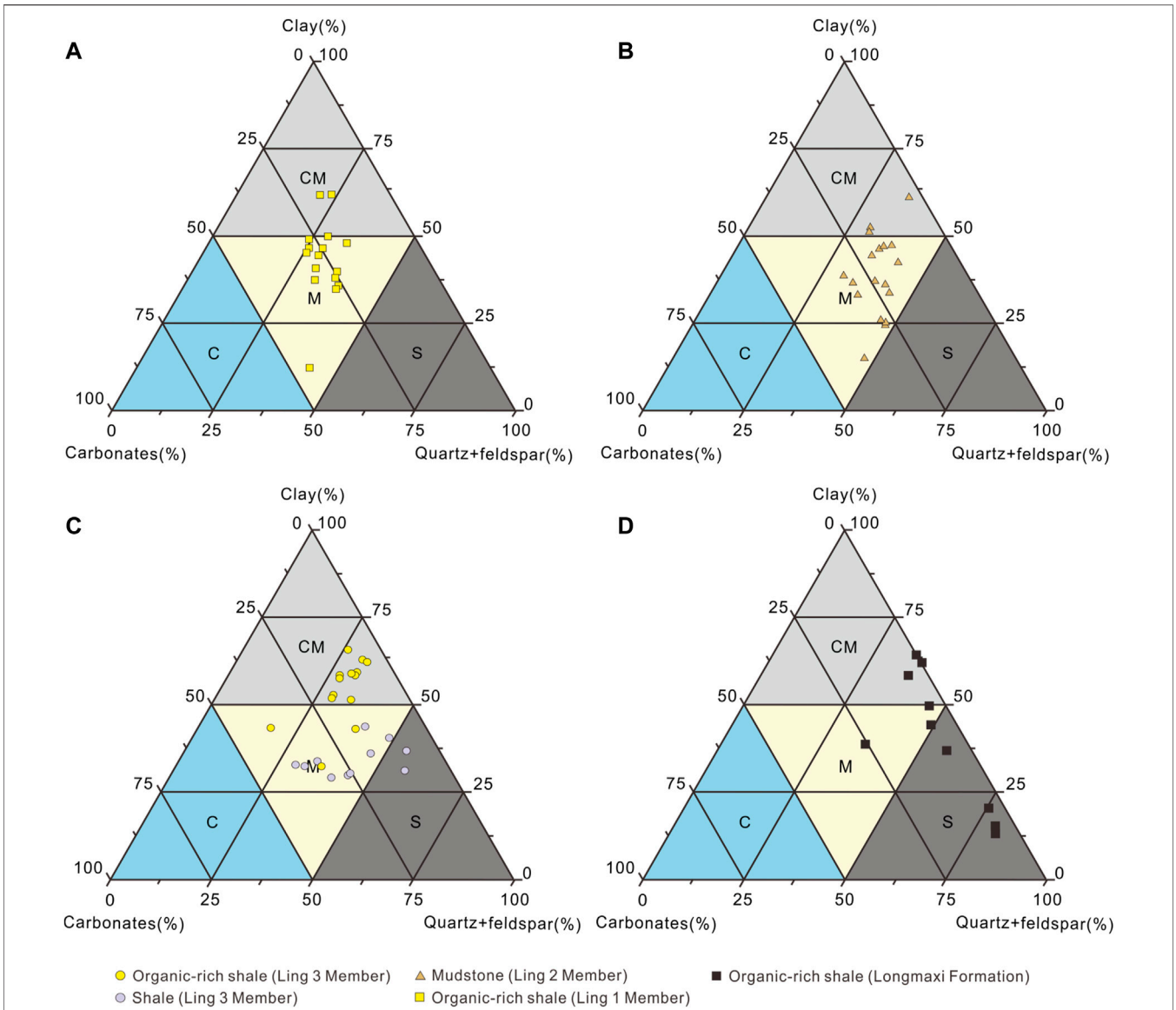

FIGURE 4 | Ternary lithofacies diagram of the Upper Permian Linghao Formation shale/mudstone samples. CM: argillaceous shale; M: mixed shale; S: siliceous shale; C: carbonate shale. **(A)** Organic-rich shale, Ling 1 member. **(B)** Mudstone, Ling 2 member. **(C)** Organic-rich shale and shale, Ling 3 member. **(D)** Organic-rich marine shale, Longmaxi Formation (Jia et al., 2020).

contains a small amount of solid bitumen (**Figure 2**), which provides a material basis for exploring the maturity of organic matter in this area (**Figures 2E,F**). Based on comparative thermal simulation experiments and natural evolution samples, Wang et al. (2020) pointed out that when the vitrinite reflectance is greater than 1.5%, the solid bitumen reflectance is approximately equal to the vitrinite reflectance. Highly mature to overmature shale can be evaluated directly by solid bitumen reflectance. The results suggest that the overall bitumen reflectivity of Linghao Formation is high (n = 5), with an average value of 3.85%. The thermal maturity of organic matter can be equivalent to vitrinite reflectivity. It is found that the thermal maturity of the Ling 1 member is significantly higher than that of the other two members (**Table 1**), which is speculated to be related to the volcanic activity represented by basalt interbed.

Organic carbon isotope is mainly controlled by the source of organic matter and remains stable during the thermal evolution of geological history. It is generally used for the evaluation of organic matter types in overmature shales. The carbon isotope of kerogen ($\delta^{13}C_{kerogen}$) in Linghao Formation ranges from -22.2‰ to -20.3‰ (n = 6). The carbon isotopes of Ling 1 kerogen range from -20.3‰ to -20.4‰. The carbon isotopes of kerogen in Ling 2 member mudstone are between -21.9‰ and -22.1‰. The carbon isotopes of kerogen in Ling 3 member organic-rich shale range from -22.2‰ to -22.1‰.

TABLE 2 | TOC content and mineralogical composition of the Upper Permian Linghao Formation shale/mudstone from studied well.

Rock Fabrics	Depth (m)	TOC (%)	Quartz (%)	Feldspar (%)	Total clay (%)	Calcite (%)	Dolomite (%)	Siderite (%)
Shale (Ling 3)	3,291	0.24	20	9.6	30.3	30.4	2.2	0.7
Shale (Ling 3)	3,295	0.43	19.2	7.8	30.3	17.9	15.8	1.2
Shale (Ling 3)	3,299	0.85	21.3	9.4	30.7	22.8	5.5	0.7
Shale (Ling 3)	3,303	0.67	23.8	11.8	38.2	7.3	4.2	1.5
Shale (Ling 3)	3,323	0.35	32.1	6.4	28.2	25.5	3.5	0.8
Shale (Ling 3)	3,326	0.55	42.8	11.2	29.8	6.7	2.9	1.4
Shale (Ling 3)	3,329	1.25	29.5	16.1	38.3	6.7	2.4	1.2
Shale (Ling 3)	3,331	0.98	36.7	15.8	35.8	4.6	2.5	0.9
Shale (Ling 3)	3,349	0.50	30.9	11.1	29.2	19.5	4	0.8
Shale (Ling 3)	3,353	0.74	31.1	12.7	34.7	7	9.3	0.5
Shale (Ling 3)	3,357	0.58	33.8	7.4	28.6	7.9	16.2	0.8
Organic-rich shale (Ling 3)	3,383	1.78	10.8	5.1	38.8	15.1	18.1	1.8
Organic-rich shale (Ling 3)	3,391	3.56	16.7	12.2	54.9	1.1	7.3	1.7
Organic-rich shale (Ling 3)	3407.32	4.36	14.9	9.8	45.9	1.3	8.8	6.3
Organic-rich shale (Ling 3)	3408.92	3.33	16.4	13.8	58.6	1.2	1.1	3.2
Organic-rich shale (Ling 3)	3412.12	2.57	15.3	12.6	55.4	0.1	8.5	2
Organic-rich shale (Ling 3)	3414.87	3.86	14.3	9.5	61.6	2.5	3.9	1.9
Organic-rich shale (Ling 3)	3,418	2.47	13.9	12.5	55.2	1.6	11.1	1.6
Organic-rich shale (Ling 3)	3,422	2.18	14.2	12.4	48.6	6.9	10.2	1.3
Organic-rich shale (Ling 3)	3,426	3.18	16.5	11.6	57.7	0.7	3.9	1.4
Organic-rich shale (Ling 3)	3,430	2.28	15.2	10.4	54.5	1.9	10.1	1.7
Organic-rich shale (Ling 3)	3,459	3.44	15.2	14.5	56.6	0.1	8	1.2
Organic-rich shale (Ling 3 member)	3,463	2.00	18.9	18.4	41.4	0.8	16.4	0.3
Organic-rich shale (Ling 3)	3,467	2.27	14.1	17.7	48.8	0.7	12.2	1.5
Organic-rich shale (Ling 3)	3,471	1.90	12.2	21	30	1	25.3	3.4
Mudstone (Ling 2)	3,481	1.57	28.6	7.9	34.8	10.5	11.6	0.6
Mudstone (Ling 2)	3,485	2.38	17.7	10.9	48.2	2.5	14	0.9
Mudstone (Ling 2)	3,489	2.60	18.3	13.2	40.8	3.9	14.2	1.4
Mudstone (Ling 2)	3,493	3.08	17.4	10.2	48.2	1.7	11.7	2.8
Mudstone (Ling 2)	3,497	2.92	19	16.6	44.5	0.7	12.4	0.9
Mudstone (Ling 2)	3556.95	1.27	25.6	8.6	44.8	0.3	14.8	1
Mudstone (Ling 2)	3557.35	0.63	26.5	15.9	24.1	1.4	23.6	1.1
Mudstone (Ling 2)	3557.75	1.82	10.9	21	55.4	0.5	1.5	1.2
Mudstone (Ling 2)	3,561	0.50	14.8	16.4	33.9	0.5	26.5	0.8
Mudstone (Ling 2)	3563.15	1.29	31.2	13.6	22.9	18.2	6.8	1
Mudstone (Ling 2)	3,596	1.91	17.2	23.9	31.4	1.3	18.5	1
Mudstone (Ling 2)	3,608	1.18	16.4	22.9	34	0.9	18.6	1.1
Mudstone (Ling 2)	3,631	1.49	25.1	13.6	39.2	9.7	3.4	1.3
Mudstone (Ling 2)	3,676	0.60	17.3	16.8	30.8	23.2	3.9	1.1
Mudstone (Ling 2)	3,705	0.83	15.1	13.9	37.1	25.6	3.3	0.8
Mudstone (Ling 2)	3,726	0.99	20.3	12.6	43.4	6.8	9.3	1.2
Mudstone (Ling 2)	3,729	1.37	23.7	19.1	22.7	1.5	19.1	4.2
Mudstone (Ling 2)	3,732	0.96	29.8	14.7	13.9	13	20.7	1.6
Organic-rich shale (Ling 1)	3,752	0.84	28.1	11	10.9	21.2	17.8	1.7
Organic-rich shale (Ling 1)	3,754	2.23	14	15.1	34.5	10	18.1	0.6
Organic-rich shale (Ling 1)	3,756	2.73	12.6	15.6	38.2	7.9	18.2	1.2
Organic-rich shale (Ling 1)	3,758	3.30	11.6	15.2	41.3	8.7	14.9	1.2
Organic-rich shale (Ling 1)	3,760	4.12	9.7	14.1	42.1	8.2	17.3	1.7
Organic-rich shale (Ling 1)	3765.14	2.80	9.5	11.7	56.1	1.6	10.3	1.4
Organic-rich shale (Ling 1)	3767.54	1.86	14.4	12.2	46.3	0.9	17.9	1.1
Organic-rich shale (Ling 1)	3770.74	3.57	7.4	11.3	55.9	2.6	11.7	1.6
Organic-rich shale (Ling 1)	3772.24	3.13	18.7	15	35.3	1	20.8	2
Organic-rich shale (Ling 1)	3,775	1.96	22.5	8.6	43.8	2.3	12.8	1.2
Organic-rich shale (Ling 1)	3,802	2.36	20.6	6.4	43.4	12.8	8.8	1.3
Organic-rich shale (Ling 1)	3,804	2.71	13.6	19.5	36.9	11.4	10.1	1
Organic-rich shale (Ling 1)	3,806	3.60	13.6	8.7	44.8	9.3	13.6	1.5
Organic-rich shale (Ling 1)	3,809	2.91	15.5	8.2	43.4	8	16.5	1.5
Organic-rich shale (Ling 1)	3,811	2.19	25	10.1	32.1	7.3	16.3	1.5
Organic-rich shale (Ling 1)	3,813	0.94	20.1	16.6	34.4	9.1	15.1	0.7

According to the relative enrichment of 12C ($\delta^{13}C_{kerogen}$ < -28‰) in Linghao Formation kerogen, it is suggested that the organic matter of Linghao Formation is composed of type I kerogen (Wang et al., 2002; Hu et al., 2019). The kerogen maceral identification suggested that the sapropel asphaltene content in the organic-rich shale of the Linghao Formation is

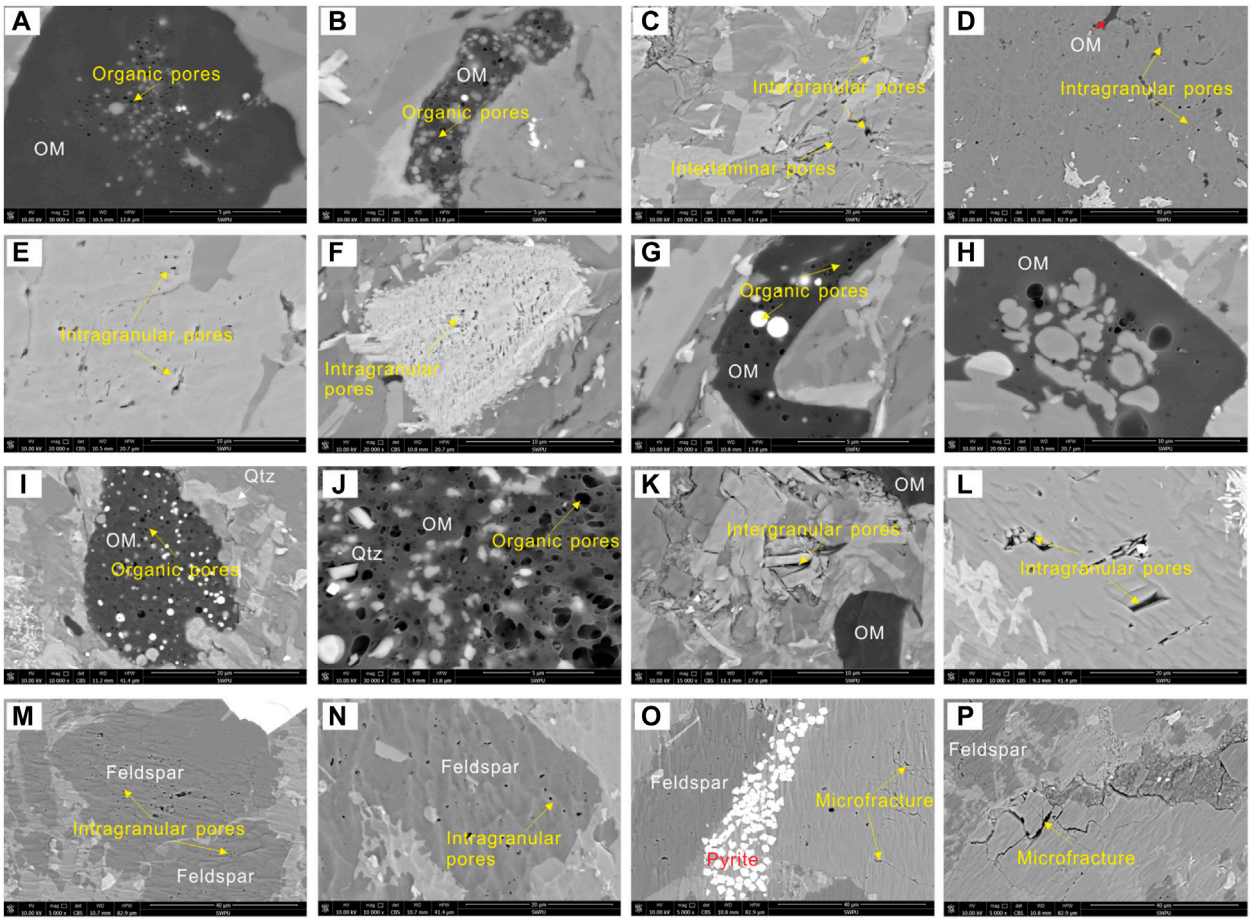

FIGURE 5 | High-resolution SEM image of Upper Permian Linghao Formation shale/mudstone. **(A,B)** Organic pores in a single OM grain of organic-rich shale, Ling 1 member, 3,772.40 m. **(C,D)** Organic-rich shale, Ling 1 member, 3,770.30 m **(E)** Intragranular pores of dissolution origin in mudstone, Ling 2 member, 3,556.80 m. **(F)** Intragranular pores of dissolution origin in mudstone, Ling 2 member, 3,558.48 m. **(G)** Mudstone, Ling 2 member, 3,558.48 m. **(H)** Mudstone, Ling 2 member, 3,556.80 m. **(I,J)** Abundant organic pores in organic matter–inorganic mineral complex of organic-rich shale, Ling 3 member, 3,407.00 m. **(K,L)** Organic-rich shale, Ling 3 member, 3,407.00 m. **(M,N)** Intragranular pores of dissolution origin in feldspar grain, shale, Ling 3 member, 3,261.82 m. **(O,P)** Microfractures in clay mineral, shale, Ling 3 member, 3,261.82 m

relatively high (**Figure 2**), and it is often filled in the pore spaces of authigenic minerals or contacted with authigenic minerals, showing irregular morphology. The maceral of organic matter is mainly composed of sapropel (n = 6), the proportion is between 90 and 96% with an average value of 93.83%. The solid bitumen content is relatively low, ranging from 4 to 10%.

Shale is a kind of fine-grained sedimentary rock, and its material composition is complex. The inorganic mineral types are mainly terrigenous minerals or authigenic minerals. Mineral composition reflects the material source of the reservoir, which has an impact on shale gas reservoir space, gas adsorption, fracture development, post-fracturing fracture, and process performance. It is an important part of shale reservoir evaluation. Results suggest that Ling 1 member organic-rich shale is characterized by a clay content of 40.0% (10.9–56.1%), quartz content of 16.1% (7.4–28.1%), feldspar content of 12.5% (6.4–19.5%), and carbonate content of 24.0% (13.3–40.7%) (**Figure 3A**). Ling 2 member mudstone is characterized by a clay content of 36.1% (13.9-55.4%), quartz content of 20.8% (10.9–31.2%), feldspar content of 15.1% (7.9–23.9%), and carbonate content of 21.1% (3.2–35.3%) (**Figure 3B**). Organic-rich shale in the lower part of Ling 3 member is characterized by a clay content of 50.6% (30.0–61.6%), quartz content of 14.9% (10.8–18.9%), feldspar content of 13.0% (5.1–21.0%), and carbonate content of 14.9% (5.5–35.0%). Shale in the upper part of Ling 3 member is characterized by a clay content of 32.2% (28.2–38.3%), quartz content of 29.2% (19.2–42.8%), feldspar content of 10.8% (6.4–16.1%), and carbonate content of 21.4% (8.0–34.9%) (**Figures 3C,D**).

The ternary diagram plotting mineralogy clearly shows that compared to Longmaxi Formation marine shales (Jia et al., 2020), the Permian Linghao Formation shales is not similar to these marine shales in terms of mineral

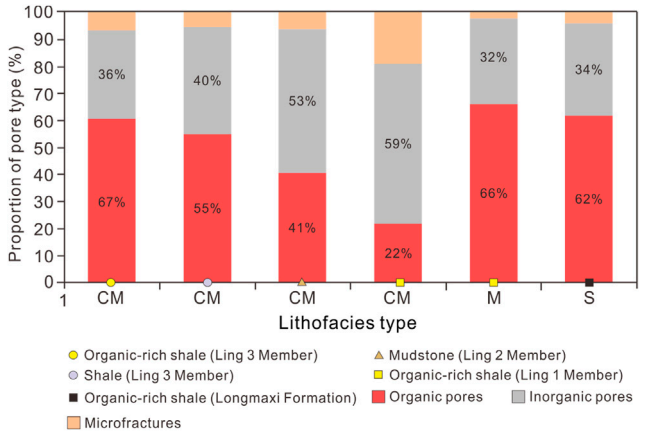

FIGURE 6 | High-resolution SEM image processing technology showing reservoir space proportion in Upper Permian Linghao Formation shale/mudstone.

composition (**Figure 4**). Siliceous shale (S) lithofacies is not developed in Linghao Formation (**Table 2**). Ling 1 member organic-rich shale is mainly mixed shale (M) lithofacies, but some samples are argillaceous shale (CM) lithofacies (**Figure 4A**). The mudstone of Ling 2 is similar to the lithofacies of Ling 1 member (**Figure 4B**). The upper part of Ling 3 member is mainly composed of mixed shale lithofacies (M), while the organic-rich shale in the lower part of Ling 3 is mainly composed of argillaceous shale (CM) (**Figures 4C,D**).

Reservoir Space Types

Analysis of SEM images using image processing technology is used in the study (**Figure 5**). Results suggest that microfractures are well developed in argillaceous shale (CM) lithofacies of Lin 1 organic-rich interval, accounting for 19% and organic pores for only 22% (**Figure 5**). The proportion of reservoir space types of mixed shale lithofacies (M) is very similar to marine shale (**Figure 6**). The lithofacies are dominated by organic pores, accounting for 66%. The proportion of organic pores is 41% in argillaceous shale (CM) lithofacies of Ling 2 member mudstone. The proportion of reservoir space types in argillaceous shale (CM) lithofacies of Ling 3 member is very similar to that of marine shale and argillaceous shale (CM) lithofacies of Lin 1 member. The lithofacies are dominated by organic pores, accounting for 67%. The proportion of organic pores in argillaceous shale (CM) lithofacies of Lin 3 member is 55% (**Figure 6**).

Porosity Characteristics

The porosity of Ling 1 member organic-rich shale ranges from 0.11 to 1.01%, with an average of 0.52% (n = 9). The porosity of Ling 2 member mudstone ranges from 0.17 to 2.26%, with an average of 1.22% (n = 8). The porosity of Ling 3 member organic-rich interval ranges from 0.94 to 2.38%, with an average of 1.99% (n = 17). The porosity of Ling 3 member shale ranges from 0.83 to 1.07%, with an average of 0.95% (n = 2).

Pore Size Distribution (PSD)

In order to reveal the pore size distribution of Linghao Formation, the NMR cryoporometry PSD curve was combined with SEM observation. The PSD curve shows a bimodal shape in Ling 1 member organic-rich shale, with peaks at 3–6 nm and 8–11 nm, respectively (**Figures 7A,B**), corresponding to the nano-scale organic pores (**Figures 5A,B**). Meanwhile, pores ranging from 11 to 110 nm contribute a little to pore volume, corresponding to inorganic pores and a small amount of microfractures (**Figures 5C,D**). The PSD curve of Ling 2 member mudstone is similar to that of Ling 1 member organic-rich shale (**Figures 7C,D**). The pore volume is mainly composed of 2- to 3-nm and 4- to 11-nm micropores, corresponding to a large number of nano-sized intragranular dissolved pores in feldspar (**Figures 5E,F**). Meanwhile, 11- to 90-nm inorganic pores and microfractures also contribute to the pore volume. A few organic pores with pore size larger than 100 nm contribute little to the pore volume (**Figures 5G,H**). The PSD curve shows a singlet shape in Ling 3 member organic-rich shale (**Figures 7E,F**). The pore volume is mainly composed of 2- to 3-nm and 4- to 11-nm micropores. The micropores at 3–10 nm also make a small contribution to the pore volume, and these micropores correspond to organic pores. Organic pores with larger pore size (**Figures 5I,J**), inorganic pores, and microfractures contribute little to pore volume in Ling 3 member organic-rich shale (**Figures 5K,L**). The PSD curve shows a singlet shape in Ling 3 member shale (**Figures 7G,H**). The pore volume is mainly composed of inorganic pores of about 2 nm, and inorganic pores of 3–10 nm also have a small contribution (**Figures 5M,N**). The contribution of large inorganic pores and microfractures to the pore volume is not obvious (**Figures 5O,P**).

The Content of Desorbed Gas

Adsorption capacity of shale is the most important factor controlling total gas content of shale. Curtis. (2002) proposed that adsorbed shale gas accounted for 20–85% of the total shale gas content. Li et al. (2007) suggested that the adsorbed shale gas content accounted for at least 40%. The isothermal adsorption experiment is one of the most important measurements to obtain the shale gas content. At 110°C, the excess adsorption capacity increased first and then decreased with the increase in pressure. The excess adsorption capacity of methane increased rapidly with the increase in pressure in the low-pressure stage. When the adsorption amount reaches the peak, the excess adsorption amount will gradually decrease with the continuous increase in pressure, which is the essential feature of excess adsorption amount of supercritical methane (Zhou et al., 2016). Results suggest that the absolute adsorption gas content of the two samples from Ling 1 member organic-rich shale are 1.21 m^3/t and 1.64 m^3/t, respectively (**Figures 8A,B**). The absolute adsorption gas content of Ling 2 member mudstone is 0.78 m^3/t and that of Ling 3 member organic-rich shale is 1.14 m^3/t (**Figures 8C,D**). The absolute adsorption gas content of Ling 1 and Ling 3 organic-rich shale exceed the minimum standard for

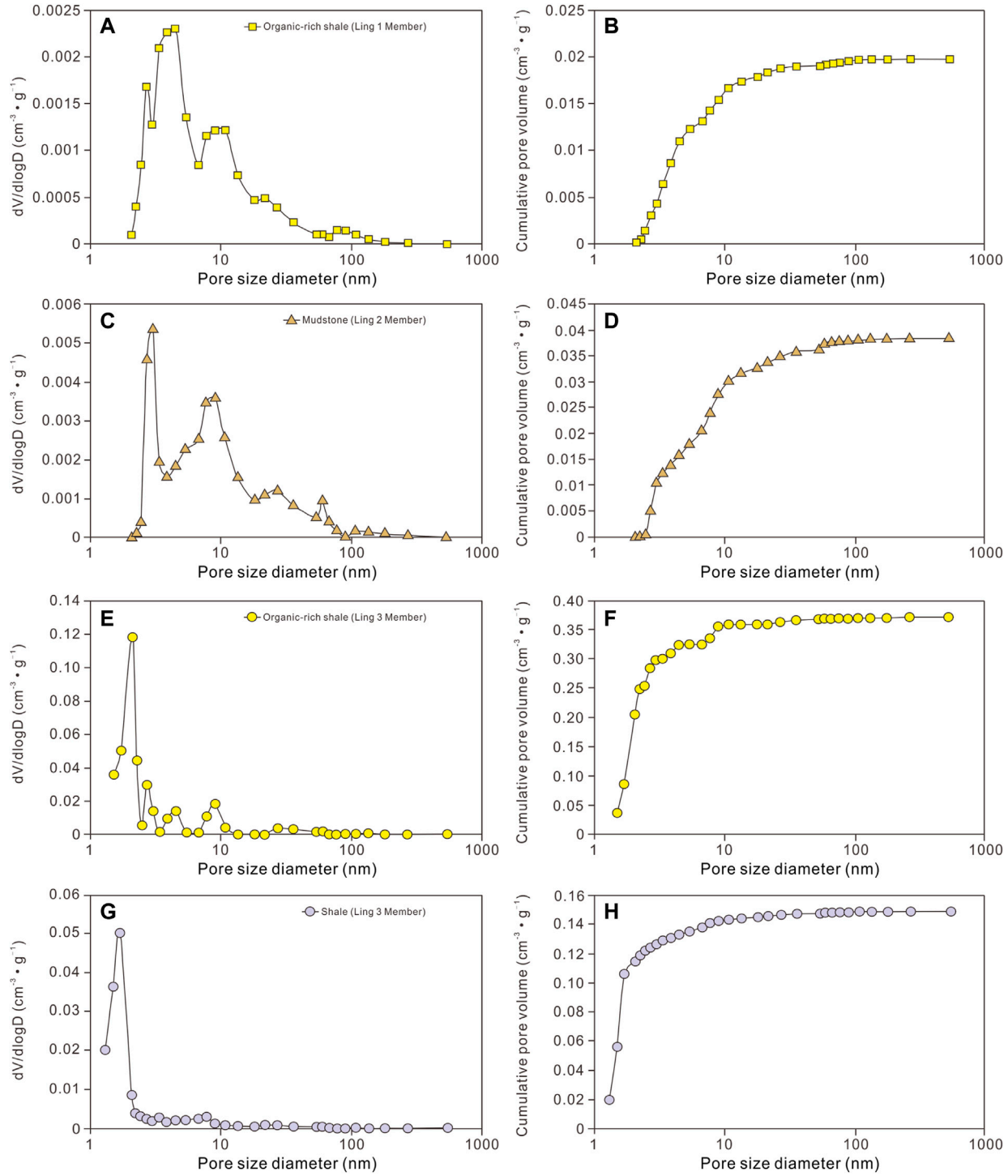

FIGURE 7 | NMR cryoporometry pore size distribution curves for the Upper Permian Linghao Formation shale/mudstone from the studied well in Nanpanjiang Basin. **(A)** Ling 1 member organic-rich shale, 3,772.05 m. **(B)** Ling 1 member organic-rich shale, 3,772.05 m. **(C)** Ling 2 member mudstone, 3,556.80 m. **(D)** Ling 2 member mudstone, 3,556.80 m. **(E)** Ling 3 member organic-rich shale, 3,407.00 m. **(F)** Ling 3 member organic-rich shale, 3,407.00 m. **(G)** Ling 3 member shale, 3,410.50 m. **(H)** Ling 3 member shale, 3,410.50 m.

commercial shale gas development in China (1.0 m^3/t) (Zhang J. et al., 2012). Previous studies have shown that adsorbed gas in marine shale accounts for 20–50% of the total gas content, with an average of 34% (Pang et al., 2019). According to the adsorption gas ratio of 50%, the total gas content of Ling 1 and Ling 3 organic-rich shale can reach 3.28 m^3/t and 2.28 m^3/t,

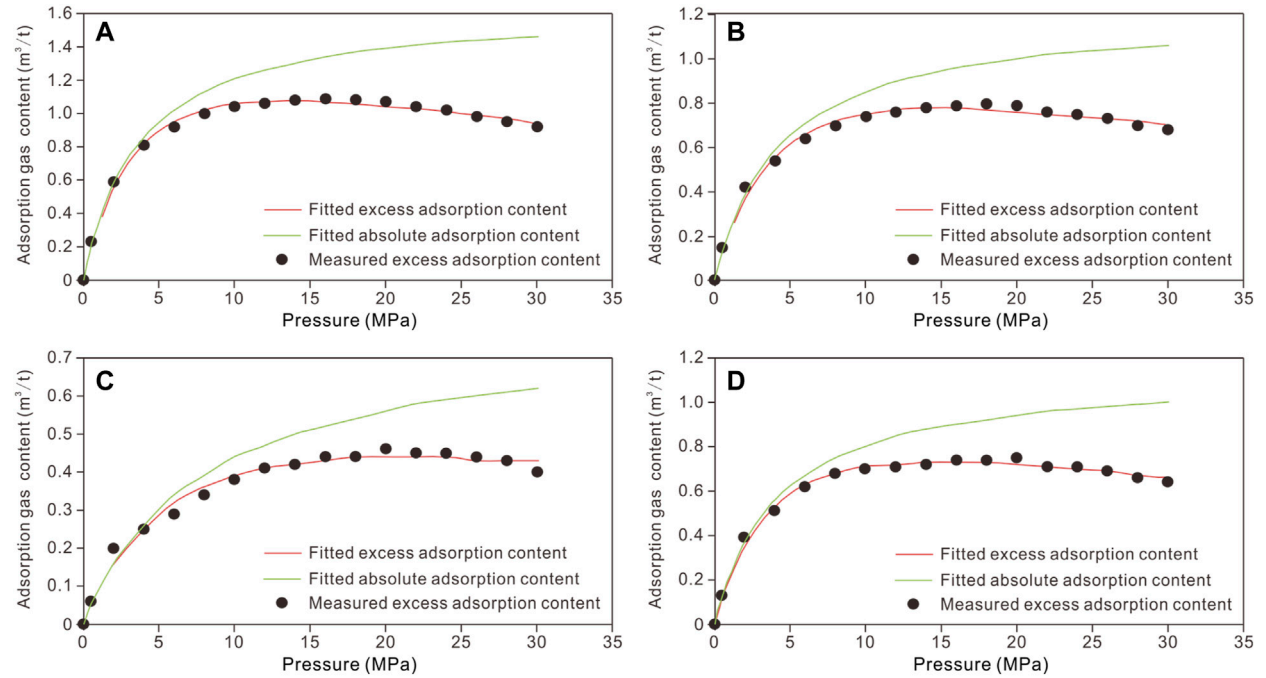

FIGURE 8 | Methane isothermal adsorption results for the Upper Permian Linghao Formation shale/mudstone from the studied well in Nanpanjiang Basin. **(A)** Organic-rich shale, Ling 1 member, 3,767.54 m. **(B)** Organic-rich shale, Ling 1 member, 3,772.24 m. **(C)** Mudstone, Ling 2 member, 3,557.75 m. **(D)** Organic-rich shale, Ling 3 member, 3,412.12 m

respectively. It is suggested that the Upper Permian Linghao Formation shale in the Nanpanjiang Basin has a significant potential for shale gas exploration.

CONCLUSION

1) Twosets of organic-rich shales developed in the Upper Permian Linghao Formation, which are the Ling 1 member and the lower part of Ling 3 member, respectively. The Linghao organic-rich shales are predominantly characterized by kerogen type I, with a relatively highly mature to overmature status. High remaining TOC and high to overmaturity indicate that Linghao organic-rich shales have generated significant amounts of gas and can be a good shale gas reservoir.
2) The Ling 1 member organic-rich shale is mainly a mix of shale lithofacies, but some samples are argillaceous shale lithofacies. The Ling 2 member mudstone is similar to the argillaceous shale lithofacies of Ling 1 member. The upper part of Ling 3 member is mainly composed of mixed shale lithofacies, while the organic-rich shale in the lower part of Ling 3 is mainly composed of argillaceous shale.
3) The pore volume in Ling 1 organic-rich shale is mainly contributed by 3- to 6-nm and 8- to 11-nm organic pores. The pore volume of Ling 2 mudstone is mainly composed of 2- to 3-nm and 4- to 11-nm intragranular dissolved pores in feldspar. Then 11- to 90-nm inorganic pores and microfractures also contribute evidently to the pore volume. The pore volume of Ling 3 organic-rich shale is mainly composed of 2- to 3-nm and 4- to 11-nm organic pores. The organic pores between 3 and 10 nm also have a small contribution to the pore volume. The pore volume in Ling 3 shale is mainly composed of inorganic pores of about 2 nm, and inorganic pores of 3–10 nm also make a small contribution.
4) Theabsolute adsorption gas content of Ling 1 organic-rich shale is 1.21 m^3/t or 1.64 m^3/t. The absolute adsorption gas content of Ling 2 mudstone is 0.78 m^3/t and that of Ling 3 organic-rich shale is 1.14 m^3/t. The absolute adsorption gas content of Ling 1 and Ling 3 organic-rich shale exceeds the minimum standard for commercial shale gas development in China (1.0 m^3/t). According to the adsorption gas ratio of 50%, the total gas content of Ling 1 and Ling 3 organic-rich shale can reach 3.28 and 2.28 m^3/t, respectively. It is suggested that the Upper Permian Linghao Formation shale in the Nanpanjiang Basin has a significant potential for shale gas exploration.

DATA AVAILABILITY STATEMENT

The original contributions presented in the study are included in the article/Supplementary Material, further inquiries can be directed to the corresponding author.

AUTHOR CONTRIBUTIONS

YG contributed as the major author of the article. DH conceived the project. ZW, RL and JH collected the samples. ZF, JH, GC and YJ analyzed the samples. All authors have contributed to the article and approved the submitted version.

FUNDING

This study was funded by the National Science and Technology Major Project of China (Grant number 2017ZX05036) and Science and Technology Cooperation Project of the CNPC-SWPU Innovation Alliance (Grant No. 2020CX030101).

REFERENCES

Alalade, B., and Tyson, R. V. (2013). Influence of Igneous Intrusions on thermal Maturity of Late Cretaceous Shales in the Tuma Well, Chad Basin, NE Nigeria. *J. Afr. Earth Sci.* 77, 59–66. doi:10.1016/j.jafrearsci.2012.09.006

Bao, S., Lin, T., Nie, H., and Ren, S. (2016). Preliminary Study of the Transitional Facies Shale Gas Reservoir Characteristics: Taking Permian in the Xiangzhong Depression as an Example. *Earth Sci. Front.* 23 (1), 44–53. doi:10.13745/j.esf.2016.01.004

Cao, T., Song, Z., Wang, S., and Xia, J. (2015). Physical Property Characteristics and Controlling Factors of Permian Shale Reservoir in the Lower Yangtze Platform. *Nat. Gas Geosci.* 26 (2), 341–351. doi:10.11764/j.issn.1672-1926.2015.02.0341

Chen, F., Wei, X., Liu, Z., Ao, M., and Yan, J. (2020). Pore Development Characteristics and Main Controlling Factors of the Permian marine-continent Transitional Shale in the Sichuan Basin. *Nat. Gas Geosci.* 31 (11), 1593–1602. doi:10.11764/j.issn.1672-1926.2020.04.028

Clarkson, C. R., Jensen, J. L., and Chipperfield, S. (2012). Unconventional Gas Reservoir Evaluation: What Do We Have to Consider? *J. Nat. Gas Sci. Eng.* 8, 9–33. doi:10.1016/j.jngse.2012.01.001

Ding, J., Zhang, J., Shi, G., Shen, B., Tang, X., Yang, Z., et al. (2021). Sedimentary Environment and Organic Matter Enrichment Mechanisms of the Upper Permian Dalong Formation Shale, Southern Anhui Province, China. *Oil&gas Geology*. 42 (1), 158–172. doi:10.11743/ogg20210114

Ding, J., Zhang, J., Tang, X., Huo, Z., Han, S., Lang, Y., et al. (2018). Elemental Geochemical Evidence for Depositional Conditions and Organic Matter Enrichment of Black Rock Series Strata in an Inter-platform basin: the Lower Carboniferous Datang Formation, Southern Guizhou, Southwest China. *Minerals* 8 (11), 509. doi:10.3390/min8110509

Guo, X., Hu, D., Liu, R., Wei, X., and Wei, F. (2018). Geological Conditions and Exploration Potential of Permian marine-continent Transitional Facies Shale Gas in the Sichuan Basin. *Nat. Gas Industry* 38 (10), 11–18. doi:10.3787/j.issn.1000-0976.2018.10.002

Han, J., Chen, B., Zhao, X., Zheng, C., and Zhang, J. (2017). Development Characteristics and Influential Factors of Organic Pores in the Permian Shale in the Lower Yangtze Region. *Nat. Gas Industry* 37 (10), 17–26. doi:10.3787/j.issn.1000-0976.2017.10.003

He, Q., Dong, T., He, S., Zhai, G., Guo, X., Hou, Y., et al. (2020). Sedimentological and Geochemical Characterization of the Upper Permian Transitional Facies of the Longtan Formation, Northern Guizhou Province, Southwest China: Insights into Paleo-Environmental Conditions and Organic Matter Accumulation Mechanisms. *Mar. Pet. Geology*. 118, 104446. doi:10.1016/j.marpetgeo.2020.104446

Hu, G., Liu, W., Luo, H., Wang, J., Chen, Q., Tengger, B., et al. (2019). The Impaction of Original Organism Assemblages in Source Rocks on the Kerogen Carbon Isotopic Compositions: a Case Study of the Early Paleozoic Source Rocks in the Tarim Basin, China. *Bull. Mineralogy, Pet. Geochem.* 38 (5), 902–913. doi:10.19658/j.issn.1007-2802.2019.38.133

Jarvie, D. M., Hill, R. J., Ruble, T. E., and Pollastro, R. M. (2007). Unconventional Shale-Gas Systems: the Mississippian Barnett Shale of north-central Texas as One Model for Thermogenic Shale-Gas Assessment. *Bulletin* 91, 475–499. doi:10.1306/12190606068

Jia, A., Hu, D., He, S., Guo, X., Hou, Y., Wang, T., et al. (2020). Variations of Pore Structure in Organic-Rich Shales with Different Lithofacies from the Jiangdong Block, Fuling Shale Gas Field, SW China: Insights into Gas Storage and Pore Evolution. *Energy Fuels* 34, 12457–12475. doi:10.1021/acs.energyfuels.0c02529

John B. Curtis1, J. B. (2002). Fractured Shale-Gas Systems. *Bulletin* 86 (11), 1921–1938. doi:10.1306/61EEDDBE-173E-11D7-8645000102C1865D

Kuang, L., Dong, D., He, W., Wen, S., Sun, S., Li, S., et al. (2020). Geological Characteristics and Development Potential of Transitional Shale Gas in the East Margin of the Ordos Basin, NW China. *Pet. Exploration Dev.* 47 (3), 435–446. doi:10.11698/PED.2020.03.0110.1016/s1876-3804(20)60066-0

Li, X., Hu, S., and Cheng, K. (2007). Suggestions from the Development of Fractured Shale Gas in North America. *Pet. Exploration Dev.* 34 (4), 392–400. doi:10.3321/j.issn:1000-0747.2007.04.002

Liang, Q., Zhang, X., Tian, J., Sun, X., and Chang, H. (2018). Geological and Geochemical Characteristics of marine-continental Transitional Shale from the Lower Permian Taiyuan Formation, Taikang Uplift, Southern North China Basin. *Mar. Pet. Geology*. 98, 229–242. doi:10.1016/j.marpetgeo.2018.08.027

Liu, Q., Li, P., Jin, Z., Liang, X., Zhu, D., Wu, X., et al. (2021). Preservation of Organic Matter in Shale Linked to Bacterial Sulfate Reduction (BSR) and Volcanic Activity under marine and Lacustrine Depositional Environments. *Mar. Pet. Geology*. 127, 104950. doi:10.1016/j.marpetgeo.2021.104950

Liu, S., Wu, C., Li, T., and Wang, H. (2018). Multiple Geochemical Proxies Controlling the Organic Matter Accumulation of the marine-continental Transitional Shale: A Case Study of the Upper Permian Longtan Formation, Western Guizhou, China. *J. Nat. Gas Sci. Eng.* 56, 152–165. doi:10.1016/j.jngse.2018.06.007

Luo, W., Hou, M., Liu, X., Huang, S., Chao, H., Zhang, R., et al. (2018). Geological and Geochemical Characteristics of marine-continental Transitional Shale from the Upper Permian Longtan Formation, Northwestern Guizhou, China. *Mar. Pet. Geology*. 89, 58–67. doi:10.1016/j.marpetgeo.2017.06.029

Nie, H., Tang, X., and Bian, R. (2009). Controlling Factors for Shale Gas Accumulation and Prediction of Potential Development Area in Shale Gas Reservoir of South China. *Acta Petrolei Sinica* 30 (4), 484–491. doi:10.3321/j.issn:0253-2697.2009.04.002

Pang, X., Chen, G., Xu, C., Tong, M., Ni, B., and Bao, H. (2019). Quantitative Evaluation of Adsorbed and Free Gas and Their Mutual Conversion in Wufeng-Longmaxi Shale, Fuling Area. *Oil Gas Geology*. 40 (6), 1247–1258. doi:10.11743/ogg20190609

Qiu, Z., and Zou, C. (2020). Controlling Factors on the Formation and Distribution of "Sweet-Spot Areas" of marine Gas Shales in South China and a Preliminary Discussion on Unconventional Petroleum Sedimentology. *J. Asian Earth Sci.* 194, 103989. doi:10.1016/j.jseaes.2019.103989

Ross, D. J. K., and Marc Bustin, R. (2009). The Importance of Shale Composition and Pore Structure upon Gas Storage Potential of Shale Gas Reservoirs. *Mar. Pet. Geology*. 26, 916–927. doi:10.1016/j.marpetgeo.2008.06.004

Simoneit, B. R. T., Brenner, S., Peters, K. E., and Kaplan, I. R. (19781978). Thermal Alteration of Cretaceous Black Shale by Basaltic Intrusions in the Eastern Atlantic. *Nature* 273 (5663), 501–504. doi:10.1038/273501a0

Sun, M., Zhang, L., Hu, Q., Pan, Z., Yu, B., Sun, L., et al. (2019). Pore Connectivity and Water Accessibility in Upper Permian Transitional Shales, Southern China. *Mar. Pet. Geology*. 107, 407–422. doi:10.1016/j.marpetgeo.2019.05.035

Sun, M., Zhao, J., Pan, Z., Hu, Q., Yu, B., Tan, Y., et al. (2020). Pore Characterization of Shales: A Review of Small Angle Scattering Technique. *J. Nat. Gas Sci. Eng.* 78, 103294. doi:10.1016/j.jngse.2020.103294

Wang, J., Chen, J., Wang, D., and Zhang, S. (2002). Study on the Characteristics of Carbon Isotopic Composition and Hydrocarbon Generation Potential of Organic Matter of Middle-Upper Proterozoic in Northern Part of North China. *Pet. Exploration Dev.* 29 (5), 13–15. doi:10.3321/j.issn:1000-0747.2002.05.004

Wang, X., Li, B., Yang, X., Wen, L., Xu, L., Xie, S., et al. (2021). Characteristics of "Guangyuan-Wangcang" Trough during Late Middle Permian and its Petroleum Geological Significance in Northern Sichuan Basin, SW China. *Pet. Exploration Dev.* 48 (3), 562–574. doi:10.11698/PED.2021.03.1110.1016/s1876-3804(21)60052-6

Wang, X., Mou, C., Xiao, Z., Zheng, B., Chen, Y., Wang, Q., et al. (2018). Genesis of Black Rock Series of Upper Permian Dalong Formation in Hefeng Area, Hubei Province: an Evidence from the Analysis of Element Geochemistry in Well HD1. *Acta Petrolei Sinica* 39 (12), 1355–1369. doi:10.7623/syxb201812004

Wang, Y., Qiu, N., Ma, Z., Ning, C., Zheng, L., Zhou, Y., et al. (2020). Evaluation of Equivalent Relationship between Vitrinite Reflectance and Solid Bitumen Reflectance. *J. China Univ. Mining Tech.* 49 (3), 563–575. doi:10.13247/j.cnki.jcumt.001114

Wang, Z., Guo, B., Jiang, C., Qi, L., Jiang, Y., Gu, Y., et al. (2022). Nanoscale Pore Characteristics of the Lower Permian Shanxi Formation Transitional Facies Shale, Eastern Ordos Basin, North China. *Front. Earth Sci.* 10, 842955. doi:10.3389/feart.2022.842955

Wei, H., Chen, D., Wang, J., Yu, H., and Tucker, M. E. (2012). Organic Accumulation in the Lower Chihsia Formation (Middle Permian) of South China: Constraints from Pyrite Morphology and Multiple Geochemical Proxies. *Palaeogeogr. Palaeoclimatol. Palaeoecol.* 353-355, 73–86. doi:10.1016/j.palaeo.2012.07.005

Wei, Z., Wang, G., Wang, Y., Ma, X., Zhang, T., He, W., et al. (2020). Geochemical and Geological Characterization of Marine-Continental Transitional Shale: A Case Study in the Ordos Basin, NW China. *Acta Geologica Sinica - English Edition* 94 (3), 809–821. doi:10.1111/1755-6724.13888

Xi, Z., Tang, S., Wang, J., Yang, G., and Li, L. (2018). Formation and Development of Pore Structure in marine-continental Transitional Shale from Northern China across a Maturation Gradient: Insights from Gas Adsorption and Mercury Intrusion. *Int. J. Coal Geology*. 200, 87–102. doi:10.1016/j.coal.2018.10.005

Xi, Z., Tang, S., Zhang, S., Lash, G. G., and Ye, Y. (2022). Controls of marine Shale Gas Accumulation in the Eastern Periphery of the Sichuan Basin, South China. *Int. J. Coal Geology*. 251, 103939. doi:10.1016/j.coal.2022.103939

Xi, Z., Tang, S., Zhang, S., and Sun, K. (2017). Pore Structure Characteristics of Marine-Continental Transitional Shale: A Case Study in the Qinshui Basin, China. *Energy Fuels* 31, 7854–7866. doi:10.1021/acs.energyfuels.7b00911

Xia, W., Yan, Q., Xiang, Z., Xia, L., Jiang, W., Wei, W., et al. (2018). Sedimentary Characteristics of the Early-Middle Triassic on the South Flank of the the Xilin Faulted Block in the Nanpanjiang basin and its Tectonic Implications. *Acta Petrologica Sinica* 34 (7), 2119–2139.

Zhang, C., Chen, H., Chen, A., Lin, L., Long, K., and Yang, S. (2012b). Sedimentary System Distribution and Evolution of Permianin South Guizhou-Middle Guangxi, China. *J. Chengdu Univ. Tech. (Science& Tech. Edition)* 39 (6), 643–650.

Zhang, C., Chen, H., Lin, L., and Chen, A. (2012c). Sedimentary Filling Characteristics and Evolution Process from Permian to Middle Triassic in South Guizhou and Middle Guangxi. *Geology. China* 39 (2), 414–425.

Zhang, J., Li, X., Zhang, X., Zhang, M., Cong, G., Zhang, G., et al. (2018). Geochemical and Geological Characterization of marine-continental Transitional Shales from Longtan Formation in Yangtze Area, South China. *Mar. Pet. Geology*. 96, 1–15. doi:10.1016/j.marpetgeo.2018.05.020

Zhang, J., Lin, L., Li, Y., Jiang, S., Liu, J., Jiang, W., et al. (2012a). The Method of Shale Gas Assessment: Probability Volume Method. *Earth Sci. Fronties* 19 (2), 184–191. doi:10.1016/j.energy.2013.05.031

Zhang, K., Jia, C., Song, Y., Jiang, S., Jiang, Z., Wen, M., et al. (2020a). Analysis of Lower Cambrian Shale Gas Composition, Source and Accumulation Pattern in Different Tectonic Backgrounds: A Case Study of Weiyuan Block in the Upper Yangtze Region and Xiuwu Basin in the Lower Yangtze Region. *Fuel* 263 (2020), 115978. doi:10.1016/j.fuel.2019.115978

Zhang, K., Jiang, S., Zhao, R., Wang, P., Jia, C., and Song, Y. (2022). Connectivity of Organic Matter Pores in the Lower Silurian Longmaxi Formation Shale, Sichuan Basin, Southern China: Analyses from Helium Ion Microscope and Focused Ion Beam Scanning Electron Microscope. *Geol. J.* 1–13. doi:10.1002/gj.4387

Zhang, K., Peng, J., Liu, W., Li, B., Xia, Q., Cheng, S., et al. (2020b). The Role of Deep Geofluids in the Enrichment of Sedimentary Organic Matter: a Case Study of the Late Ordovician-Early Silurian in the Upper Yangtze Region and Early Cambrian in the Lower Yangtze Region, south China. *Geofluids* 2020, 1–12. doi:10.1155/2020/8868638

Zhang, K., Peng, J., Wang, X., Jiang, Z., Song, Y., Jiang, L., et al. (2020c). Effect of Organic Maturity on Shale Gas Genesis and Pores Development: A Case Study on marine Shale in the Upper Yangtze Region, South China. *Open Geosciences* 12 (2020), 1617–1629. doi:10.1515/geo-2020-0216

Zhang, K., Song, Y., Jia, C., Jiang, Z., Jiang, S., Huang, Y., et al. (2019b). Vertical Sealing Mechanism of Shale and its Roof and Floor and Effect on Shale Gas Accumulation, a Case Study of marine Shale in Sichuan basin, the Upper Yangtze Area. *J. Pet. Sci. Eng.* 175, 743–754. doi:10.1016/j.petrol.2019.01.009

Zhang, K., Song, Y., Jiang, S., Jiang, Z., Jia, C., Huang, Y., et al. (2019a). Mechanism Analysis of Organic Matter Enrichment in Different Sedimentary Backgrounds: A Case Study of the Lower Cambrian and the Upper Ordovician-Lower Silurian, in Yangtze Region. *Mar. Pet. Geology*. 99, 488–497. doi:10.1016/j.marpetgeo.2018.10.044

Zhou, S., Wang, H., Xue, H., Guo, W., and Lu, B. (2016). Difference between Excess and Absolute Adsorption Capacity of Shale and a New Shale Gas reserve Calculation Method. *Nat. Gas Industry* 36 (11), 12–20. doi:10.3787/j.issn.1000-0976.2016.11.002

Zhu, W., Zhang, X., Zhou, D., Fang, C., Li, J., and Huang, Z. (2021). New Cognition on Pore Structure Characteristics of Permian marine Shale in the Lower Yangtze Region and its Implications for Shale Gas Exploration. *Nat. Gas Industry* 41 (7), 41–55. doi:10.3787/j.issn.1000-0976.2021.07.005

Zou, C., Dong, D., Wang, S., Li, J., Li, X., Wang, Y., et al. (2010). Geological Characteristics and Resource Potential of Shale Gas in China. *Pet. Exploration Dev.* 37 (6), 641–653. doi:10.1016/s1876-3804(11)60001-3

Zou, C., Dong, D., Wang, Y., Li, X., Huang, J., Wang, S., et al. (2015). Shale Gas in China: Characteristics, Challenges and Prospects (I). *Pet. Exploration Dev.* 42 (6), 753–767. doi:10.1016/S1876-3804(15)30072-0-012

Zou, C., Zhu, R., Chen, Z.-Q., Ogg, J. G., Wu, S., Dong, D., et al. (2019). Organic-matter-rich Shales of China. *Earth-Science Rev.* 189, 51–78. doi:10.1016/10.1016/j.earscirev.2018.12.002

Conflict of Interest: Authors DH, ZW, RL, JH, ZF, and JH were employed by Exploration Company of Sinopec.

The remaining authors declare that the research was conducted in the absence of any commercial or financial relationships that could be construed as a potential conflict of interest.

Publisher's Note: All claims expressed in this article are solely those of the authors and do not necessarily represent those of their affiliated organizations or those of the publisher, the editors, and the reviewers. Any product that may be evaluated in this article, or claim that may be made by its manufacturer, is not guaranteed or endorsed by the publisher.